Semnan University

Mechanics of Advanced Composite Structures

journal homepage: http://MACS.journals.semnan.ac.ir

Artificial Intelligence Method for Predicting Mechanical Properties of Sand/Glass Reinforced Polymer: a New Model

M. Heshmati[a], S. Hayati [a*], S. Javanmiri[a], M. Javadian[b]

[a] *Department of Mechanical Engineering, Kermanshah University of Technology, Kermanshah, 67156-85420, Iran*
[b] *Department of Computer Engineering, Kermanshah University of Technology, Kermanshah, 67156-85420, Iran*

KEYWORDS

Reinforced polymer
Mechanical properties
A new model
Active learning method
Neural networks

ABSTRACT

In this paper, the aim is to propose a new model to obtain the mechanical properties of sand/glass polymeric concrete including modulus of elasticity and the ultimate tensile stress. The neural network soft computation, support vector machine (SVM), and active learning method (ALM) that is a fuzzy regression model are all used to construct a simple and reliable model based on experimental datasets. The experimental data are obtained via the tensile and bending tests of sand/glass reinforced polymer with different weight percentages of sand and chopped glass fibers. The extracted results are then used for training and testing of the neural network models. Two different types of neural networks including feed-forward neural network (FFNN) and radial basis neural network (RBNN) are employed for connecting the properties of the sand/glass reinforced polymer to the properties of the resin and weight percentages of sand and glass fibers. Besides the neural network models, the SVM and ALM models are applied to the problem. The models are compared with each other with respect to the statistical indices for both train and test datasets. Finally, to obtain the properties of the sand/glass reinforced polymer, the most accurate model is presented as an FFNN model.

1. Introduction

In the last decades, polymeric concrete (PC) has been widely used for new constructions and repairing old constructions due to its good properties, such as rapid setting, high strength, corrosion, and water resistance. Polymer concrete (PC) is fabricated generally by combining the polymers and the fillers. The resin, (e.g. epoxy or polyester) plays the role of a binder instead of cement binders in plain concretes [1]. The unsaturated isophthalic and orthophthalic polyesters can be used as a binder in PC at special conditions such as harsh environments like acid or alkaline media or water [2]. Moreover, epoxy resins are widely used for the manufacturing of polymer concretes due to their suitable mechanical properties and especially their high binding resistance.

Because of the adhesion of the polymeric concrete, repairing both polymer and conventional cement-based concretes are possible. Polymer concrete is an ideal material for underground constructions because of its neutral chemical structure and water impermeability. Conducted studies about mechanical behaviors of such materials under chemical attack situations certify their performance in such situations [3, 4]. While cement-bound mortars cannot resist to chlorine-based acids and the effects of sulfate, polymer-based mortars show resistance both as repair mortar or coating. Polymer concrete also shows good resistance to water and has a high hydraulic capacity thanks to its smoothness [5]. Their adhesion property is the most important property of these materials as they are widely used to reinforce concrete structures [6-12].

Several research works have been conducted for determining the material characteristics of different types of polymer concrete [13-16]. Abdel-Fattah and El-Hawary [17] conducted experiments to study the flexural behavior of polymer concrete (PC) made with epoxy resin and polyester with varying percentages. The results show that the modulus of rupture and ultimate compressive strain for PC were much higher. Thus, the ductility was improved in

* Corresponding author. Tel.: +98-9127616631
E-mail address: s.hayati@kut.ac.ir

DOI: 10.22075/MACS.2020.20699.1268
Received 20-06-24; Received in revised form 20-08-08; Accepted 20-12-01

comparison with the ordinary Portland cement concrete. Komendant et al. [18] investigated the effect of testing temperature on the compressive strength as well as the influence of thermal cycling between 23 and 71 0C on the strength and elastic properties of concrete. They observed that the compressive strength of the concrete is reduced by 3–11% at 43 0C and 11–21% at 71 0C. However, only a few articles have been published in the literature which consider the effect of environment conditions on the PC properties. In some other works [19-22] a numerical analysis approach was used to investigate the mechanical properties of concrete.

Since the PC exhibits brittle failure behavior, improving its post-peak stress-strain behavior is an important aspect for the application of PC. Hence, developing better PC systems and also characterizing the fracture properties and flexural strength in terms of constituents are essential for the efficient use of PC [23, 24]. Chopped strand glass fiber has been applied to polymer composites for improving the strength and controlling the cracking [25, 26]. Thus, before being used in practical and industrial applications, the study of their mechanical properties is necessary. To characterize the failure behavior of the polymer composites with respect to the constituents, some attempts have been made for efficient use [27] or optimizing the mechanical properties [28, 29].

However, since these materials are newly developed, the study of their mechanical properties is much necessary before using them in practical and industrial applications. Analytical methods such as numerical homogenization are used to determine composite material properties [30]. The microstructure interpolation method is also applied for multiple length scale structural optimization [31]. In addition, Akbari et al [32] applied a multi-scale method based on the homogenization technique to investigate the influence of microscopic parameters on the macroscopic behavior of polycrystalline materials under different loading configurations. Since there is still no mathematical model to obtain the mechanical properties of PCs in general, most of the research work on the mechanical properties are limited to experimental studies [33-41]. Thus, the only way for estimation of the mechanical properties of a PC is through a time consuming and expensive experimental process.

Therefore, in this study, the artificial intelligence (AI) soft computation modeling based on experimental data is chosen to construct a simple and reliable model for the estimation of mechanical properties of the PCs. As an example, Shabani and Mazaheri used the artificial neural network models in numerical modeling of nano-sized ceramic particulates reinforced metal matrix composites [42]. They studied the accuracy of various artificial neural network training algorithms in FEM modeling of Al2O3 nanoparticles reinforced A356 matrix composites. A hybrid artificial intelligence-based model is also used to study the bond strength of CFRP-lightweight concrete composites [43].

The tensile and bending test specimens of sand/glass reinforced polymer concrete with different weight percentages of sand/glass are fabricated. Modulus of elasticity and the ultimate tensile stress are obtained via the tensile and bending tests. The extracted results are then used for training and testing of the neural network models. Different types of neural networks including feed-forward neural network (FFNN), radial basis neural network (RBNN) beside the support vector machine (SVM), and active learning method (ALM) are employed for connecting the properties of the sand/glass reinforced PC to the properties of the resin and weight percentages of sand and chopped glass. All the models are fitted to the problem properly with acceptable accuracy. Finally, a model is presented as a simple formula based on the FFNN structure to obtain the mechanical properties of the sand/glass reinforced PC.

Instead of using expensive experimental studies for the estimation of sand/glass reinforced polymers properties, the presented model can easily be used via any programming software. The presented scheme can also be used for the study of any other complicated material.

2. Methodology

In this section, the utilized methods for obtaining the experimental results and constructing the artificial intelligence (AI) models are discussed. At first, each value of modulus of elasticity for the composite (E_c) or ultimate stress for the composite (σ_{uc}) is experimentally obtained with respect to three parameters including the modulus of elasticity for the resin (E_r) or ultimate stress for the resin (σ_{ur}), the weight percentage of sand (%sand), and weight percentage of chopped glass fiber (%glass) in the composite structure. In order to obtain stiffness and ultimate compressive strength of the composite, E_c or σ_{uc} for each certain value of E_r or σ_{ur}, %sand, and %glass, ten specimens with similar configurations are made for tensile and bending tests. Therefore, every result is derived as an average result of 5 tensile tests and 5 bending tests. The results for E_c and σ_{uc} are obtained for 240 different configurations

(as tabulated in Tables A-1, 2, 3, and 4), which means there are over 2400 tests performed to obtain the presented results.

In the next step, the obtained results are used to construct the neural network models. Two separate networks are founded in every section, one for estimation of E_c with respect to E_r, wt% of sand, and wt% of glass fiber, and another for estimation of σ_{uc} with respect to σ_{ur}, wt% of sand, and wt% of glass fiber. The modulus of elasticity for both resin and composite (E_r and E_c) are in GPa and the ultimate tensile stresses for both resin and composite (σ_{ur} and σ_{uc}) are in MPa. The datasets are divided into two categories consisting of train and test datasets. For the below explained structures of the utilized neural networks, the components of the networks, including weight and bias terms, are acquired via an optimization process to fit the training dataset results in the training procedure. After the training procedure, the network should be tested over the test datasets. The testing observation datasets are not used in training and preserved for testing the generality of the neural network model. The same procedure of training and testing is performed for the ALM model as well. The generality of a method means that the method should give proper results for any other data other than the training data. In this study, 80% of the results are taken as the training datasets (192 observations) and the rest are left for testing of the networks (48 observations). A flow chart of the computational procedure is shown in Fig. 1.

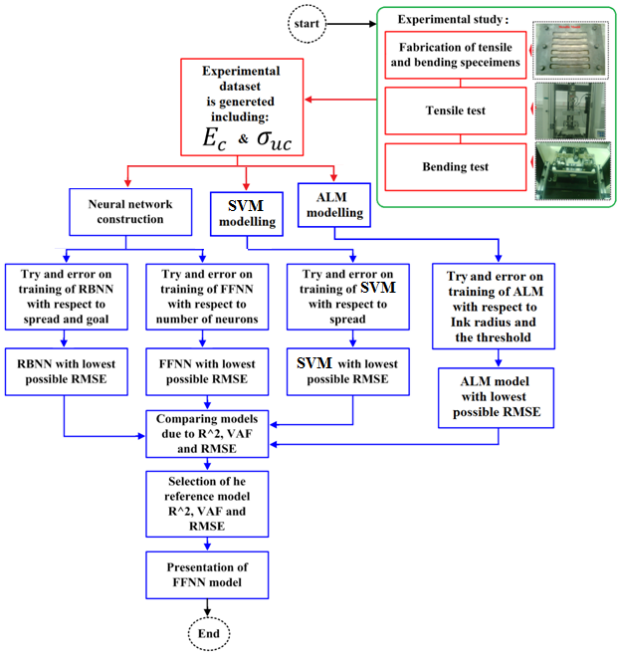

Fig. 1. A flow chart for prediction of mechanical properties of polymer concrete

Fig. 2. The fabricated metallic mould

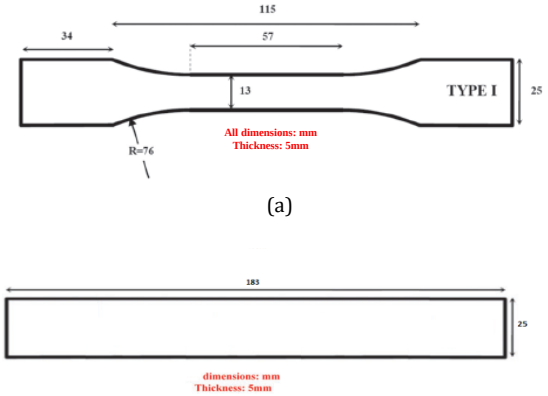

Fig. 3. Dimensions of the (a) tensile and (b) bending samples

2.1. Experimental Setup

Different types of resins including EPON 828, EPON 862, Epoxy L135i, LY564, and PVA are used to fabricate the test specimens. Sand particles and chopped glass fibers are also used for reinforcement of test specimens. The sand is sieved by two different sieves so all the grains of sand are about 2-4 mm in diameter and also all strands of chopped glass fiber are about 6mm in length.

The preparation of specimens is the most important stage of any testing method. The American Society for Testing and Materials (ASTM) has a tensile test standard designed to determine the tensile properties of unreinforced and reinforced plastics in the form of standard dumbbell (dog-bone) shaped test specimens. The tensile test specimen has the basic shape of a tensile dog bone according to ASTM D 638 (Type I). The dimensions of the specimen are 168mm in length, 13mm in width, and 5mm in thickness (Figs. 2-3).

After preparing the materials, the mould should be prepared, so the process of preparing the mould is as follow:

Fig. 4. Removal of specimens from the stainless steel mould

- Assembling the mould and making sure that both upper and lower parts are well attached.
- Using a suitable lubricant (machine oil, grease, or any commercially available mould release agent) to avoid the sticking of samples on the mould.
- Setting the fabricated mould on the flat surface so that the mould does not move during casting the epoxy mixture.
- Adding sand and chopped glass fiber into the cavities of the mould if necessary.

The next step is preparing the matrix, as mentioned; the matrix is a mixture of resin epoxy, and hardener, so at the beginning, these two materials are mixed well and stirred for more than 5min then the mixture is sonicated in the ultrasonic bath for more than 15min. this process helps the removal of almost all of the bubbles from the matrix so a uniform mixture will be achieved. When a uniform mixture of the resin and hardener is provided, the epoxy mixture must be poured into the cavities on the stainless steel mould. Then the mould should be placed in the oven to cure the samples for 5h at 55°C. Finally, the specimens are ready to be removed from the stainless steel mould, but there might be some unwanted extensions on the contour of the specimens that need to be removed before testing (Fig.4).

When it comes to the testing set up and execution, according to conducted tensile and bending tests, two methods, one for tensile tests and the other one for bending tests, are necessary to follow. Figs. 5 and 6 illustrate the experimental setup for both tensile and bending tests.

For the tensile tests, dog-bone specimens are placed in the top and bottom grips and tightened while one visually observes alignment of the long axis of the specimen with the direction of the pull and for bending tests, the specimen is placed on the two lower edges and the third edge on the top moves down until the specimen is broken. Tensile and bending test specimens are fabricated with different sand and chopped glass fiber weight fractions: 0% to 55% with increments of 5% for sand, and 0% to 15% with increments of 5% for chopped glass fiber. Both tensile and bending tests are performed at room temperature under a crosshead speed of 5mm/min. In addition, it is necessary to be mentioned that for each weight percentage, five tensile and one bending test samples are prepared to achieve more reliable results.

As seen in Appendix A, the specimens with 55% sand have a higher stiffness than other samples. According to this appendix, the ultimate tensile strength for the sample that contains 20% of sand is 5.1637MPa. By increasing the weight percentage of sand, the ultimate tensile strength increases significantly and for specimens containing 40% and 55%, the ultimate tensile strength is 5.6995MPa and 7.1863MPa, respectively. However, for samples that contain 20% and 40% of sand, the Young's modulus doesn't change widely but for 55% sand specimen, young's modulus is about 2.5 times higher than 20% and 40% sand specimens.

To study the effect of chopped glass fiber on the ultimate tensile strength of polymers and also to find out about the influence of increasing the amount of chopped glass fiber on the ultimate tensile strength of specimens, two different amounts of chopped glass fiber are mixed with pure polymer. Tables A-1 to A-4 also include information about the samples having specific amount of chopped glass fiber. As illustrated, by adding 5% extra chopped glass fiber to the polymer, its ultimate tensile strength increases about 30% and as expected in comparison with sand contained specimens, the chopped glass fiber samples have a higher ultimate tensile strength.

The simultaneous influence of adding chopped glass fiber and sand particles is also investigated. Two different percentages are presented in the table; the first specimen contains 40% sand and the second one contains a mixture of 40% sand and 5% chopped glass fiber. According to the presented results in Appendix A, adding 5% of chopped glass fiber can increase the ultimate tensile strength up to 60%. Also, the amount of young's modulus increases from 1.82GPa to 3.50GPa by adding 5% glass fiber into specimens.

2.2. Feed-Forward Neural Network (FFNN)

Feed-forward neural networks (FFNN) are the most primary neural networks. The FFNNs are successfully utilized to model nonlinear problems or estimate complicated functions. The FFNN is usually used as a simple numerical instrument to estimate the results of complicated phenomena after being trained. The structure may have multiple hidden layers but usually, it consists of one hidden layer and one

output layer. Multiple layers may lead to extra complication of the network that causes problems in the training procedure and convergence. The structure of an FFNN with one hidden layer is depicted in the Fig. 5. Note that the shown inputs and output of the system belong to the estimation of the mechanical properties of the sand/glass polymer composite.

The input data should be pre-processed before it is entered into the hidden layer. The pre-processing is a linear transform that maps the minimum and maximum of input data ([x_{min}, x_{max}]) into the domain between -1 and 1 ([-1, 1]). In the hidden layer, the mapped input data is multiplied by a weight matrix (W_h) and added to a bias vector (b_h). This summation is then applied by a tangent sigmoid (*tansig*) transfer function. Note that the weight matrix of W_h in the hidden layer is a $N_n \times N_i$ matrix of real numbers where N_n is called the number of neurons in the hidden layer and N_i is the dimension of the input vector or the number of input parameters that is equal to 3 for this problem. As mentioned above, the three input parameters of the network are E_r or σ_{ur}, %sand, and %glass. The bias vector of b_h in the hidden layer is also an $N_n \times 1$ vector of real numbers. The number of neurons is an important factor in a neural network that significantly affects both the accuracy and complexity of that network and it will be discussed later.

In the output layer, a similar process is applied to the output of the hidden layer. The data is multiplied by a weight matrix (W_o) and then added to a bias vector (b_o). The transfer function of the output layer is a pure linear (*purelin*) function that gives the same value of its input as its output. The weight matrix of W_o in the output layer is a $N_o \times N_n$ matrix of real numbers and the bias vector of b_o in the output layer is a $N_o \times 1$ vector of real numbers where N_o is the number of outputs. This problem has one output (E_c or σ_{uc}), so N_o=1. Since the output of the output layer is within the domain of [-1, 1], in order to obtain the real output values a post-process is applied to its outputs. Similar to the pre-process, the post-process is a linear transform but it maps the data from [-1, 1] into the domain between minimum output value and maximum output value ([y_{min}, y_{max}]).

After the construction of the neural network structure, the network must be trained. The training process is generally an optimization process for tuning the network parameters including W_h, b_h, W_o, and b_o.

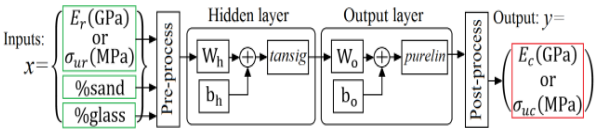

Fig. 5. The structure of a single layer FFNN model proposed for estimation of mechanical properties of sand/glass polymer composites

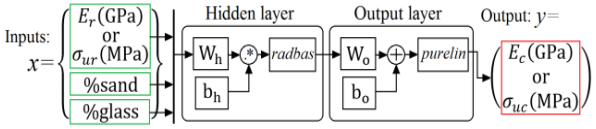

Fig. 6. The structure of an RBNN model proposed for estimation of mechanical properties of sand/glass polymer composites

During the training optimization process, the goal is to find a set of network components which minimizes the mean square error (MSE) between the network results and the real results of the training datasets. The MSE value is strictly relevant to the root mean square (RMSE). Training is done with semi-analytical backpropagation approaches such as Levenberg-Marquardt (LM) and Bayesian regularization (BR) or numerical approaches such as genetic algorithm (GA) and particle swarm optimization (PSO).

2.3. Radial Basis Neural Network (RBNN)

The structure of a radial basis neural network (RBNN) is shown in Fig. 6 which looks so similar to a single layer FFNN. The first difference is in the type of the hidden layer transfer function that is a radial basis function. In addition, in the hidden layer, an element by element multiplication operator (.*) is applied to the output of the weight matrix and the bias vector. Moreover, in the structure of RBNNs the pre-process and post-process functions return their input values.

The RBNNs take a lot of neurons, but they are easily designed and trained. RBNN gives excellent results when a lot of training data are available. The training of an RBNN is processed by adding neurons. In an exact RBNN, the number of neurons is equal to the number of input data vectors.

2.4. Support Vector Machine (SVM)

Support vector machine (SVM) is an artificial intelligence method that is widely used for classification and regression problems and it is also known as support vector regression (SVR) method. In this method, an approximate function (f(x)) is trained to fit the training dataset using a minimization method.

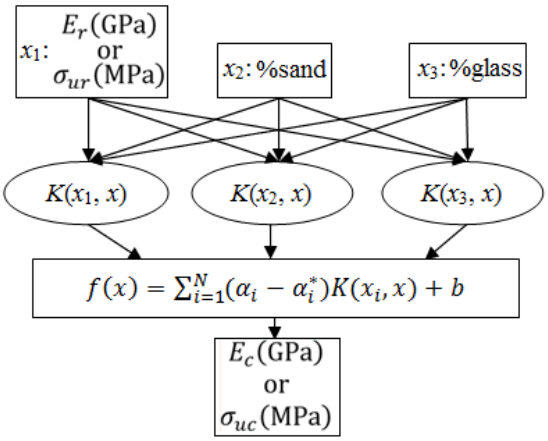

Fig. 7. The structure of an SVM model proposed for estimation of mechanical properties of sand/glass polymer composites

The structure of the constructed support vector machine in this study is illustrated in Fig. 7 which takes the resin properties (E_r or σ_{ur}) and weight percentages of sand and glass as inputs and gives the mechanical properties of the sand/glass polymer resin composites (E_c or σ_{uc}) as the output. In Fig. 7, the parameters α_i and α_i^* are the Lagrangian multipliers, N is the number of observations and $K(x_i, x)$ is the kernel function.

2.5. Active Learning Method (ALM)

ALM is a fuzzy regression algorithm, which works well in uncertain environments [44]. The basic idea of this algorithm is breaking a Multiple Input-Multiple Output (MIMO) system into several simpler Single Input-Single Output (SISO) subsystems as shown in Fig. 8.(a). Afterward, the algorithm combines these subsystems by a fuzzy inference engine in order to achieve the overall behavior of the system. Fig. 8.(b) shows a SISO subsystem of the ALM algorithm called Ink-Drop-Spread (IDS), where two valuable information (Narrow-Path and Spread)are extracted from it. Narrow-Path (NP) and Spread (SP) extracted from each SISO subsystem are then combined by a fuzzy inference unit. Equation (1) shows how these pieces of information are combined. Parameter Ψ_{ij} is the NP of each SISO subsystem and$\beta_{ij}$is the confidence degree of the NP and can be computed by Eq.(2). The ALM algorithm also considers the uncertainty for each data point by using a fuzzy membership function called an ink, as shown in fig. 8.(c). Fig. 8.(d) shows the ink drop spread of 7 data points in an IDS unit. It also shows NP and SP resulted from the IDS unit.

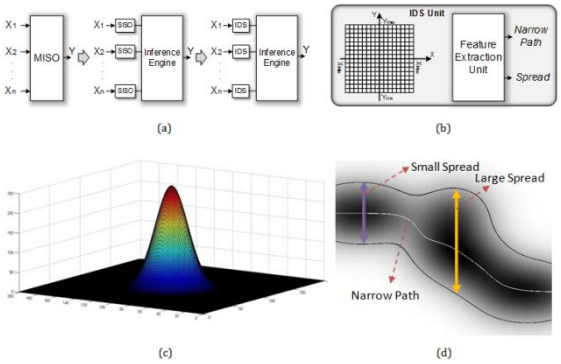

Fig. 8. (a) ALM algorithm breaks a multi-input-single-output function into simpler single-input-single output subsystems and combines the results by a fuzzy inference engine. (b) Each single-input-single-output subsystem consists of a plan called an IDS plan and a feature extractor unit which extract two useful pieces of information, Narrow Path (NP) and Spread (SP). (c) The Gaussian membership function which is called an ink. This membership function is considered for each data point in every IDS plans. (d) The inks of 7 data points are spread in an IDS plan which forms a pattern. The NP and SP are extracted from the IDS plan.

$$y(x) = \beta_{11}\Psi_{11} + \cdots + \beta_{ik}\Psi_{ik} + \cdots + \beta_{nl_n}\Psi_{nl_n} \quad (1)$$

where

$$\beta_{ij} = \frac{\frac{1}{s_{ij}}\Gamma_{ij}}{\frac{1}{s_{11}}\Gamma_{11} + \cdots + \frac{1}{s_{ij}}\Gamma_{ij} + \cdots + \frac{1}{s_{nl_n}}\Gamma_{nl_n}} \quad (2)$$

where $\frac{1}{s_{ij}}$is the Spread inverse and Γ_{ij} is the membership degree of the data point to each SISO subsystem.

The Narrow path could be obtained by the weighted-average method, as in equation (3).

$$\psi_i(x) = \{b \in Y | \sum_{y=y_{min}}^{b} d(x,y) \approx \sum_{y=b}^{y_{max}} d(x,y)\}, \quad (3)$$

where $d(x_i, y)$ is the darkness value of coordinate (x_i, y). The Spread can be computed by equation (4).

$$y(x) = \beta_{11}\Psi_{11} + \cdots + \beta_{ik}\Psi_{ik} + \cdots + \beta_{nl_n}\Psi_{nl_n} \quad (4)$$

where Th is the threshold of the IDS plane which is set by the user (usually $Th=0$ for modeling purpose).

Until now, numerous successful applications of ALM have been reported in function approximation[45, 46], classification [47-49], clustering [50, 51] and control [45, 52-54]. However, in [55] they show that ALM shows its best advantage when a high level of uncertainty existed in the system.

3. Model Construction and Evaluation

In this section, the neural network models are constructed and evaluated. The models including FFNN, RBNN, SVM, and ALM are trained and tested separately for estimation of E_c and σ_{uc}. The models are compared with each other in respect to regression plots and statistical indices such as R^2, RMSE, and VAF that are introduced below.

3.1. FFNN Results

The FFNN model is founded and trained twice, once for estimation of E_c in respect to E_r, %sand, and %glass and once for estimation of σ_{uc} in respect to σ_{ur}, %sand, and %glass. The models are trained and tested, using 192 datasets for training and 48 datasets for testing, as follows.

3.1.1. FFNN Model for Estimation of E_c

To estimate the modulus of elasticity of the sand/glass polymer composite (E_c), the FFNN model with 8 neurons in the hidden layer (N_n=8) is founded. The number of neurons is attained through a try and error procedure for finding the most exact network with the simplest structure. Hence, different numbers of neurons are applied to the network several times and the convergence of the networks is investigated noting the training and testing datasets. Finally, a single layer FFNN with 8 neurons in the hidden layer was revealed to be the most convergent network. This model also satisfies the simplicity factor with an 8×3 matrix of W_h, an 8×1 vector of b_h, a 1×8 matrix of W_o, and a 1×1 vector of b_o that generally means 26 components.

The Bayesian-regularization (BR) algorithm is used for training the network which is a fast and exact algorithm. The BR method is essentially a gradient-based method that chooses the first set of network components vector by random. Therefore, every time the BR method solves the problem, it gives different results for the network components. In order to achieve the best possible structure, the training process with the BR method is performed multiple times.

The statistical convergence indices of the finally achieved FFNN for training and testing datasets are shown in Table 1. The regression plots in Fig. 11 show the convergence between the experimental values of E_c and the FFNN results. Noting Fig. 11, the FFNN model gives proper results for both train and test datasets. Therefore, the constructed FFNN model seems to be an exact and general model for the problem. Further model evaluation is presented in the following sections.

3.1.2. FFNN Model for Estimation of σ_{uc}

To estimate the ultimate tensile stress of the sand/glass polymer composite (σ_{uc}), a similar FFNN with 11 neurons in the hidden layer is founded and trained. The statistical indices for comparison of the experimental results with the network results are given in Table 2. The same try and error procedure is applied for training the FFNN with the BR method. The indices show a proper accuracy for the network while the accuracy has a fall in comparison to the previous network.

3.2. RBNN Results

Similar to the previous section, the RBNN structure is constructed and trained once for estimation of the E_c with respect to E_r, %sand, and %glass and once for estimation of σ_{uc} in respect to σ_{ur}, %sand, and %glass. The training and testing results are primarily investigated with respect to the mentioned statistical indices.

3.2.1. RBNN Model for Estimation of E_c

For estimation of the modulus of elasticity of the composite, an RBNN with 56 neurons in the hidden layer is created. In order to reach the best accuracy, the spread value of the radial basis layer is taken equal to 10 and the goal mean squared error is taken equal to 0.01. These values for spread and goal are obtained through a try and error process.

The resulted indices for the RBNN results in comparison to the experimentally achieved composite modulus of elasticity are depicted in Table 1. The results show an excellent convergence and generality for the RBNN model.

3.2.2. RBNN Model for Estimation of σ_{uc}

A similar RBNN structure for estimation of the ultimate tensile stress of the composite is constructed with 111 neurons in the hidden layer. In order to reach the best accuracy, the spread value of the radial basis layer is taken equal to 8 and the goal mean square error is taken equal to 0.6. The values are obtained after a try and error process.

The statistical indices comparing the RBNN results with the experimentally achieved composite ultimate tensile stress are shown in Table 2. The results show an excellent convergence and a good generality for the RBNN model.

3.3. SVM Results

In this study, the Gaussian kernel function is utilized for the constructed SVM model. The parameter b is the threshold of the SVM system known as the bias term. This structure estimates the problem through an $f(x)$ function with a

deviation of ε that is a predefined parameter for accuracy and it is set to be equal to 0.001 in this study. The L1QP solver is used to solve the minimization problem that gives an SVM structure with a set of 192×3 support vectors. All the mentioned SVM settings are achieved through a try and error process to give the best possible results.

3.3.1. SVM Model for Estimation of E_c

The achieved indices for comparison of SVM results with the experimentally resulted values for composite modulus of elasticity are shown in Table 1. The results show proper accuracy for both testing and training procedures.

3.3.2. SVM Model for Estimation of σ_{uc}

The indices comparing the SVM results with the experimental values of the composite ultimate tensile stress are shown in Table 2. The results show a poor convergence for the model in training and testing states despite the previous SVM model. Therefore, the SVM model seems not to be proper for this problem.

3.4. ALM Results

In this section, the ALM structure is used for estimation of the E_c with respect to E_r, %sand, and %glass, and for estimation of σ_{uc} with respect to σ_{ur}, %sand, and %glass. A primary evaluation is possible noting the regression plots.

3.4.1. ALM Model for Estimation of E_c

The achieved statistical indices for comparison of ALM results with the experimentally resulted values for composite modulus of elasticity are shown in Table 1. The results show an acceptable convergence for the model in the training domain and testing results. The number of partitions in the ALM algorithm is 4,7 and 1 for E_r, %sand, and %glass respectively. The Ink radius is also 0.085 and the threshold value is 0.01.

3.4.2. ALM Model for Estimation of σ_{uc}

The convergence indices comparing the ALM results with the experimental values of the composite ultimate tensile stress are shown in Table 2. The results show proper accuracy for both testing and training procedures. The number of partitions in the ALM algorithm is 5, 11, and 2 for E_r, %sand, and %glass respectively. The Ink radius is also 0.005 and the threshold value is 0.01.

3.5. Model Evaluation

Evaluation of the obtained models for estimation of the mechanical properties of sand/glass polymer composites is performed in this section. In this regard, the selected performance indices are R^2, RMSE, and variance account for (VAF) which their equations can be written as follows:

$$R^2 = 1 - \frac{\sum_{i=1}^{N}(y - y')^2}{\sum_{i=1}^{N}(y' - \tilde{y})^2} \quad (5)$$

$$VAF = \left[1 - \frac{Var(y - y')}{Var(y')}\right] \times 100 \quad (6)$$

$$\text{RMSE} = \sqrt{\frac{1}{N}\sum_{i=1}^{N}(y\text{-}y')^2} \quad (7)$$

where y and y′ are the predicted and measured values, respectively, $\tilde{y}$ is the mean of the y′ values and N is the total number of data. The model will be excellent if R^2 = 1, VAF =100 and RMSE = 0.

In the following subsections, the different constructed neural network models are evaluated with respect to the above-mentioned indices. With respect to the statistical indices, the most accurate models are chosen for the problem.

3.5.1. Model Evaluation for Estimation of E_c

The statistical performance indices including R^2, RMSE, and VAF for the developed neural network models for estimation of E_c are presented in Table 1. It is observed that the resulted indices for each model are presented for both training and testing datasets.

Since the testing process is much important for generality and even convergence analysis, here it is recommended to consider the testing results as the decisive factor to ascertain the most accurate models. Comparing the resulted indices show that the most accurate model is the RBNN model for estimation of E_c. This model gives an excellent convergence and generality due to both train and test results. The results of the FFNN model are in the next grade with a slight difference. However, the FFNN model still gives excellent accuracy and generality. The poorest results belong to the RBNN model which has acceptable performance for training datasets but it doesn't give proper results for testing datasets.

Table 1. R^2, RMSE, and VAF results of the developed models for estimation of E_c

Method	State	R^2	VAF	RMSE
FFNN	Training	0.9980	99.7944	0.1008
	Testing	0.9976	99.7621	0.1073
RBNN	Training	0.9981	99.8113	0.0966
	Testing	0.9929	99.2118	0.1970
SVM	Training	0.9707	96.5334	0.4219
	Testing	0.9249	90.8253	0.6911
ALM	Training	0.9330	89.6778	0.6251
	Testing	0.9068	87.9767	0.6850

3.5.2. Model Evaluation for Estimation of σ_{uc}

The statistical performance indices including R^2, RMSE, and VAF for the developed neural network models for estimation of σ_{uc} are presented in Table 2. The aforementioned statistical indices for each model are presented for both training and testing datasets.

Noting the performance indices for the testing process in Table 2, the FFNN model gives the best results for testing datasets. Whilst the RBNN model gives better results for the training process, the FFNN model seems to be the best choice for estimation of σ_{uc} and the RBNN model is in the next grade, because, as mentioned above, the testing results have higher importance. The SVM model can also be specified as the poorest model for estimation of σ_{uc}.

3.5.3. FFNN Model 5-Folds Cross Validation

The initial evaluation of models shows that the best accuracy and generality are achieved with an FFNN model. To ensure the generality of this model over all observations, a 5-fold cross validation is applied to the structure that is shown in Table 3 and 4 respectively for estimation of E_c and σ_{uc} based on mean R^2 value.

In the 5-fold cross-validation process, the 240 observations are divided into 5 independent parts including 48 observations. Afterward, the model is trained and tested for 5 times (5 folds). In each fold, one of the separated parts is taken as the test data and the other 4 parts are taken as the training data. In this way, 100% of the dataset is used for both testing and training.

Table 2. R^2, RMSE and VAF results of developed models for estimation of σ_{uc}

Method	State	R^2	VAF	RMSE
FFNN	Training	0.9909	99.0883	1.2172
	Testing	0.9904	99.0367	1.1310
RBNN	Training	0.9963	99.6287	0.7740
	Testing	0.9383	93.5807	2.9235
SVM	Training	0.92 32	91.2052	3.0487
	Testing	0.9129	90.2342	3.8952
ALM	Training	0.9455	93.7121	3.0081
	Testing	0.9357	91.5146	3.1182

Table 3. The mean R^2 results for 5-fold cross-validation of FFNN for E_c estimation

State	Mean R^2					
	Fold 1	Fold 2	Fold 3	Fold 4	Fold 5	Average
Train	0.9980	0.9981	0.9952	0.9967	0.9918	0.9960
Test	0.9976	0.9957	0.9921	0.9907	0.9911	0.9934

Table 4. The mean R^2 results for 5-fold cross-validation of FFNN model for σ_{uc} estimation

State	Mean R^2					
	Fold 1	Fold 2	Fold 3	Fold 4	Fold 5	Average
Train	0.9909	0.9881	0.9892	0.9896	0.9918	0.9899
Test	0.9904	0.9877	0.9889	0.9865	0.9911	0.9889

The 5-folds cross validation results are in a closed range. Therefore, the results certify the generality of the FFNN model.

4. Model Presentation

In the previous sections, the models are constructed and investigated in terms of convergence and generality. The best models are chosen and it is time to represent proper models for obtaining the mechanical properties of sand/glass polymer composites. Since in addition to the accuracy the simplicity is an important factor in model presentation, for both estimation problems the FFNN model is presented that has a simple structure with excellent accuracy.

4.1. Model Presentation for E_c

An FFNN model proposed for estimation of the E_c is presented in this section. As mentioned above, in an FFNN model the input vector (x) at first should be mapped from [x_{min}, x_{max}] into the [-1, 1] domain through a linear function.

Due to the observations of the problem, the domain of [x_{min}, x_{max}] can be stated as $1.636 \le E_r \le 4$ GPa, $0 \le$ %sand ≤ 55 percent, and $0 \le$ %glass ≤ 15 percent. Therefore, the mapped inputs (x_p) can be obtained as follows.

$$x_p = \text{map}\{x\} = \text{map}\begin{Bmatrix} E_r \\ \%\text{sand} \\ \%\text{glass} \end{Bmatrix} = \begin{Bmatrix} \frac{2}{(4-1.636)}(E_r - 1.636) - 1 \\ \frac{2}{(55-0)}(\%\text{sand} - 0) - 1 \\ \frac{2}{(15-0)}(\%\text{glass} - 0) - 1 \end{Bmatrix} = \begin{Bmatrix} 0.8460 * E_r - 2.3841 \\ 0.0364 * \%\text{sand} - 1 \\ 0.1333 * \%\text{glass} - 1 \end{Bmatrix} \quad (8)$$

Noting Fig. 5, the pre mapping output (y_p) that is a value between -1 and 1 is obtained as follows.

$$y_p = W_o * \left(\text{tansig}\left(\left[W_h * \{x_p\}\right] + b_h\right)\right) + b_o \quad (9)$$

The pre mapping output should then be mapped from [-1,1] into [y_{min}, y_{max}] domain where $y_{min}=E_{cmin}$= 1.5944 GPa and $y_{max}=E_{cmax}$ =

12.4596 GPa. Then the model output (E_c in GPa) will be obtained through a linear mapping as follows.

$$\begin{aligned} & y = E_c \text{ (GPa)} \\ & = \frac{12.4596-1.5944}{2}(y_p+1)+1.5944 \\ & = 5.4326y_p + 7.0270 \end{aligned} \quad (10)$$

Having the weight and bias matrices, this model can be applied to estimate the modulus of elasticity for sand/glass polymer composites (E_c) for any in-range datasets using any programming software. The weight and bias matrices are presented as follows.

$$W_h = \begin{bmatrix} -0.1341 & -0.0935 & 0.4593 \\ -0.0356 & 0.0042 & 0.5328 \\ 0.0333 & 4.7899 & 1.0925 \\ -0.1383 & 2.2498 & 0.0960 \\ -0.2129 & -11.9967 & 0.4847 \\ -0.0706 & -2.5663 & -0.1348 \\ -0.1082 & -10.2122 & 0.4645 \\ 0.0736 & 4.6377 & 0.7621 \end{bmatrix} \quad (11)$$

$$b_h = \begin{bmatrix} -0.0837 \\ 0.1209 \\ -5.6339 \\ -0.6955 \\ 5.1714 \\ 0.4561 \\ 4.5642 \\ -5.3997 \end{bmatrix} \quad (12)$$

$$W_o = \begin{bmatrix} -2.7097 \\ 2.4493 \\ 1.4125 \\ -1.4969 \\ -1.8148 \\ -1.5225 \\ 2.0322 \\ -1.9406 \end{bmatrix}^T \quad (13)$$

$$b_o = \begin{bmatrix} -1.6722 \end{bmatrix} \quad (14)$$

4.2. Model Presentation for σ_{uc}

An FFNN model proposed for estimation of the σ_{uc} is presented in this section. Similar to the previous model, at first, the input vector (x) should be mapped from [x_{min}, x_{max}] into the [-1, 1] domain through a linear function.

Due to the observations of the problem, the domain of [x_{min}, x_{max}] can be stated as 54.48≤σ_{ur}≤93.540 MPa, 0≤%sand≤55 percent, and 0≤%glass≤15 percent. Therefore, the mapped inputs (x_p) can be obtained as follows.

$$\begin{aligned} x_p &= \text{map}\{x\} = \text{map}\begin{Bmatrix} \sigma_{ur} \\ \%\text{sand} \\ \%\text{glass} \end{Bmatrix} \\ &= \begin{Bmatrix} \frac{2}{(93.541-54.477)}(\sigma_{uc}-54.477)-1 \\ \frac{2}{(55-0)}(\%\text{sand}-0)-1 \\ \frac{2}{(15-0)}(\%\text{glass}-0)-1 \end{Bmatrix} \\ &= \begin{Bmatrix} 0.0512*\sigma_{ur}-3.7891 \\ 0.0364*\%\text{sand}-1 \\ 0.1333*\%\text{glass}-1 \end{Bmatrix} \end{aligned} \quad (15)$$

Again, noting Fig. 5, the pre mapping output (y_p) that is a value between -1 and 1 is obtained via Eq. 9.

The pre mapping output should then be mapped from [-1, 1] into [y_{min}, y_{max}] domain where y_{min}=σ_{ucmin} = 7.7242 MPa and y_{max}=σ_{ucmax} = 93.540 MPa. Then the model output (σ_{uc} in MPa) will be obtained through a linear mapping as follows.

$$\begin{aligned} & y = \sigma_{uc} \text{ (MPa)} \\ & = \frac{93.5410-7.7242}{2}(y_p+1)+7.7242 \\ & = 42.9084y_p + 50.6326 \end{aligned} \quad (16)$$

Having the weight and bias matrices, this model can be applied to estimate the modulus of elasticity for sand/glass polymer composites (σ_{uc}) for any in-range datasets using any programming software. The weight and bias matrices are presented as follows.

$$W_h = \begin{bmatrix} -0.1418 & 1.7976 & -0.7100 \\ 0.1655 & -6.2824 & -1.2883 \\ -0.0849 & -6.5189 & 0.0286 \\ -0.0084 & -3.1999 & -0.3763 \\ -0.1466 & 2.7500 & -0.3602 \\ -0.3264 & -0.2938 & -0.3056 \\ 0.0389 & -1.5997 & -0.5501 \\ -0.0963 & -1.4071 & 0.2434 \\ -0.0674 & -3.6023 & 0.0420 \\ 0.0239 & 4.5180 & 0.0929 \\ 0.0666 & -3.4163 & -0.8772 \end{bmatrix} \quad (17)$$

$$b_h = \begin{bmatrix} 2.6790 \\ -8.3193 \\ 3.6719 \\ 1.0930 \\ 3.5961 \\ 0.0760 \\ 1.2687 \\ 2.0724 \\ 1.6677 \\ -1.4328 \\ 2.8525 \end{bmatrix} \quad (18)$$

$$W_o = \begin{bmatrix} 1.2044 \\ 2.5465 \\ 1.6380 \\ -1.8026 \\ -2.1773 \\ -0.5460 \\ 1.9318 \\ 1.9297 \\ -2.8197 \\ -2.0844 \\ -0.7538 \end{bmatrix}^T \quad (19)$$

$$b_o = [0.9519] \quad (20)$$

5. Conclusions

In this study, the neural network soft computation modeling based on experimental datasets is used to construct a realistic model for the prediction of mechanical properties of sand/glass polymer composites. The tensile and bending tests are conducted to obtain the modulus of elasticity and the ultimate tensile stress of sand/glass reinforced polymer composite specimens. The extracted results are then used for training and testing of the neural network models. The model is supposed to give the mechanical properties of the sand/glass polymer composite including the modulus of elasticity and ultimate tensile stress in respect to the modulus of elasticity and ultimate tensile stress of the resin and weight percentages of sand and glass in the composite. The ALM and SVM models and two different types of neural networks including FFNN and RBNN are employed for generating a realistic model. All of the models are trained to fit the problem datasets properly through a try and error procedure. The try and error process is performed to minimize the resulted RMSE value as much as possible to obtain the most acceptable configuration of each model. Then, for both training and testing data, the extracted results of ALM, FFNN, RBNN, and SVM models are compared together in terms of accuracy using the statistical indices including R^2, RMSE, and VAF. Noting the obtained statistical indices, although all the models are excellent over the training process, the FFNN model is selected as the reference model because of its accuracy over the test data and simple structure. Since the FFNN model gives the best coincidence over the test data, it has the best generality among the obtained models. Finally, the models are presented as a simple formula based on the FFNN structure to obtain the mechanical properties of the sand/glass polymer composite with an excellent agreement with the experimental results.

Appendix A

The experimentally obtained results for modulus of elasticity (E_c) and ultimate tensile stress of the sand glass resin composites (σ_{uc}) are tabulated in this section. The neural network results are also added to the tables to perform a comparison between the experimental results and the utilized neural networks. Tables A-1 and 2 give the obtained E_c from experiments and neural networks for training and testing observations.

Tables A-1. Obtained E_c from experiments and neural networks for training observations. (Continued)

Resin type	E_r	%sand	%glass	E_c (GPa)				
				Exp.	FFNN	RBNN	SVM	ALM
	1.636	0	0	1.636	1.4927	1.6348	1.6365	1.7654
	1.636	0	5	1.705	1.6266	1.6996	1.706	1.8187
	1.636	0	10	1.9529	1.8152	1.8873	1.9541	1.907
	1.636	5	0	1.6457	1.7059	1.7794	1.6477	1.8151
	1.636	5	5	1.8827	1.8651	1.8778	1.8823	1.875
	1.636	5	10	2.1895	2.0329	2.0373	1.9893	1.9538
EPON 828	1.636	5	15	1.9656	1.9646	2.0446	1.9684	1.9512
	1.636	10	0	1.8155	1.9014	1.9023	1.8277	2.0089
	1.636	10	5	2.2046	2.0897	2.0609	2.137	2.1045
	1.636	10	10	2.0862	2.2417	2.0656	2.146	2.1177
	1.636	15	0	2.0789	2.0785	2.0488	2.0254	2.2255
	1.636	15	5	2.3276	2.3052	2.356	2.3274	2.3392
	1.636	15	10	2.3643	2.4532	2.4642	2.3658	2.2972
	1.636	15	15	2.3162	2.3009	2.3186	2.3152	2.3881

Tables A-1. Obtained E_c from experiments and neural networks for training observations. (Continued)

Resin type	E_r	%sand	%glass	E_c (GPa)				
				Exp.	FFNN	RBNN	SVM	ALM
EPON 828	1.636	20	0	2.245	2.2632	2.1761	2.2429	2.4471
	1.636	20	5	2.5642	2.5512	2.648	2.5658	2.5651
	1.636	20	15	2.7865	2.5672	2.8285	2.7854	2.6601
	1.636	25	0	2.5014	2.5515	2.4875	2.5965	2.8449
	1.636	25	5	2.9997	2.9451	3.0268	3.0684	3.0332
	1.636	25	10	3.1581	3.1879	3.1646	3.2991	3.1275
	1.636	30	0	3.066	3.0856	3.0889	3.0656	3.403
	1.636	30	5	3.9092	3.6217	3.7912	3.7824	3.6614
	1.636	30	10	4	3.9508	4.1586	3.9728	3.6977
	1.636	30	15	3.848	3.8682	4.1195	4.0486	3.8228
	1.636	35	0	3.5462	3.4027	3.5498	3.376	3.9095
	1.636	35	5	4.2758	4.1809	4.1526	4.2748	4.1736
	1.636	35	10	4.3625	4.5985	4.3258	4.3623	4.1972
	1.636	35	15	4.4736	4.4864	4.2194	4.3816	4.2085
	1.636	40	5	4.6202	4.6297	4.7265	4.1006	3.988
	1.636	40	10	5.0126	5.0469	5.1909	4.135	4.0632
	1.636	45	0	2.4319	2.3287	2.4014	2.6583	2.6061
	1.636	45	5	2.9546	2.8804	2.8722	3.2647	2.9679
	1.636	45	10	3.2384	3.16	3.1016	3.3486	3.1251
	1.636	50	0	2.003	2.0588	2.1179	2.003	2.2269
	1.636	50	5	2.2553	2.4284	2.3051	2.2556	2.3456
	1.636	50	15	2.4925	2.5655	2.5276	2.4911	2.4037
	1.636	55	0	1.6061	1.6123	1.5946	1.6688	2.1605
	1.636	55	5	1.6387	1.7033	1.6929	1.6377	2.247
	1.636	55	10	1.9237	1.7721	1.8915	1.9231	2.2485
	1.636	55	15	1.5944	1.7232	1.5807	1.8692	2.3221
EPON 862	2.463	0	0	2.463	2.433	2.4684	2.4635	2.6829
	2.463	0	5	2.8439	2.6844	2.7433	2.8421	2.7985
	2.463	0	10	2.7831	2.8273	2.9291	2.9027	2.8309
	2.463	5	0	2.6704	2.6463	2.6141	2.592	2.6934
	2.463	5	5	3.001	2.937	2.9186	2.993	2.8186
	2.463	5	10	3.1178	3.0753	3.1137	3.04	2.8499
	2.463	10	0	2.8122	2.8607	2.786	2.8103	2.8909
	2.463	10	5	3.2144	3.1968	3.1687	3.2157	3.0407
	2.463	10	10	3.2564	3.339	3.2806	3.2675	3.078
	2.463	10	15	3.1478	3.0622	3.0235	3.15	2.9613
	2.463	15	5	3.449	3.4945	3.5005	3.4487	3.454
	2.463	15	10	3.5685	3.6587	3.6415	3.5677	3.5313
	2.463	15	15	3.5241	3.3683	3.3989	3.4319	3.4332
	2.463	20	5	4.0624	3.9148	3.9352	3.8574	3.9666
	2.463	20	10	4.3724	4.1381	4.2079	4.095	4.1161
	2.463	20	15	3.9014	3.8752	4.0352	3.9458	3.861
	2.463	25	0	3.8484	3.9904	3.8945	3.9737	4.1396
	2.463	25	5	4.6449	4.6171	4.6176	4.6772	4.4599
	2.463	25	10	4.9556	4.9467	4.8587	5.0171	4.6451
	2.463	25	15	4.8271	4.753	4.5417	4.8252	4.3583
	2.463	30	5	5.7803	5.6622	5.7147	5.7827	5.5543
	2.463	30	10	6.0254	6.078	6.1448	6.1539	5.6364
	2.463	30	15	5.8519	5.9008	5.986	5.8819	5.6092
	2.463	35	0	5.3066	5.4635	5.5599	5.1602	5.8282

Tables A-1. Obtained E_c from experiments and neural networks for training observations. (Continued)

Resin type	E_r	%sand	%glass	E_c (GPa)				
				Exp.	FFNN	RBNN	SVM	ALM
	2.463	35	10	6.8829	6.8376	6.7699	6.8825	6.4567
	2.463	35	15	6.5651	6.5656	6.4596	6.5632	6.1684
	2.463	40	0	5.7196	5.8664	5.5984	4.846	5.3591
	2.463	40	5	7.1168	7.1167	7.049	6.3204	6.2489
	2.463	40	10	7.6231	7.6578	7.6916	6.6002	6.3492
	2.463	40	15	7.1352	7.1898	7.3245	6.3382	5.971
	2.463	45	0	3.9122	3.7537	3.8314	3.9129	3.87
EPON 862	2.463	45	10	4.8061	4.7216	4.7564	5.3242	4.7573
	2.463	45	15	4.5947	4.5545	4.5038	5.18	3.9366
	2.463	50	5	3.652	3.6789	3.5364	3.6504	3.7142
	2.463	50	10	3.7404	3.738	3.7761	3.7385	3.834
	2.463	50	15	3.6405	3.6337	3.6358	3.6383	3.6357
	2.463	55	0	2.5412	2.4521	2.4224	2.432	3.5049
	2.463	55	10	2.6259	2.71	2.6741	2.6262	3.6745
	2.463	55	15	2.4299	2.4547	2.3685	2.4295	3.5162
	2.6	0	0	2.6	2.5812	2.6064	2.5991	2.7867
	2.6	0	10	3.1194	2.9997	3.1026	3.121	2.9346
	2.6	0	15	2.9468	2.7743	2.9128	2.9467	2.9332
	2.6	5	0	2.7303	2.7942	2.7514	2.7415	2.8477
	2.6	5	5	3.0418	3.112	3.0899	3.1824	2.9744
	2.6	5	10	3.166	3.2522	3.2901	3.2709	3.0045
	2.6	5	15	3.1216	2.9852	3.1413	3.1193	3.0188
	2.6	10	0	2.8117	3.0112	2.9313	2.9677	3.0873
	2.6	10	10	3.5155	3.5242	3.4798	3.5038	3.2769
	2.6	15	0	3.2326	3.2581	3.2099	3.1963	3.4633
	2.6	15	5	3.6653	3.6872	3.6923	3.6652	3.6542
	2.6	15	10	3.8056	3.8607	3.8405	3.8082	3.7089
	2.6	20	0	3.5402	3.6096	3.5425	3.5413	3.9113
	2.6	20	5	4.1882	4.1348	4.1551	4.1042	4.1351
	2.6	20	10	4.4512	4.3733	4.4344	4.3451	4.2332
Epoxy L135i	2.6	25	0	4.0574	4.2168	4.1284	4.1603	4.4472
	2.6	25	5	4.8616	4.8865	4.8865	4.951	4.7739
	2.6	25	10	5.1115	5.2371	5.15	5.2878	4.8772
	2.6	25	15	4.8537	5.0351	4.8293	5.0442	4.668
	2.6	30	0	5.1853	5.1736	5.0724	4.9129	5.3885
	2.6	30	5	5.9575	5.9919	6.0316	6.0648	5.8528
	2.6	30	10	6.5311	6.4291	6.4769	6.4522	5.9409
	2.6	30	15	6.4493	6.2417	6.3004	6.1406	5.9604
	2.6	35	5	6.8684	6.7632	6.8863	6.8076	6.7436
	2.6	35	10	7.1974	7.2114	7.1748	7.1968	6.8096
	2.6	35	15	6.8498	6.9184	6.836	6.8509	6.644
	2.6	40	5	7.3229	7.5166	7.4234	6.5443	6.6028
	2.6	40	15	7.5562	7.6067	7.7255	6.6157	6.2004
	2.6	45	0	4.0099	3.9852	4.0569	4.0114	4.2799
	2.6	45	5	4.7793	4.6979	4.7659	5.298	4.9381
	2.6	45	15	4.8507	4.7917	4.7711	5.4058	4.2691
	2.6	50	5	3.7119	3.8832	3.74	3.7827	3.8905

Tables A-1. Obtained E_c from experiments and neural networks for training observations. (Continued)

Resin type	E_r	%sand	%glass	E_c (GPa)				
				Exp.	FFNN	RBNN	SVM	ALM
LY564	2.6	50	10	3.8912	3.9507	3.9765	3.9225	3.946
	2.6	50	15	3.822	3.8189	3.8267	3.7955	3.8779
	2.6	55	0	2.5189	2.5835	2.5612	2.5216	3.7452
	2.6	55	5	2.7755	2.8163	2.6968	2.7768	3.723
	2.6	55	15	2.4778	2.5839	2.5091	2.5291	3.738
	3.43	0	5	3.9318	3.8859	3.9613	3.9317	3.9038
	3.43	0	10	4.1389	4.0647	4.1465	4.1375	3.981
	3.43	0	15	3.6576	3.706	3.7671	3.6572	3.808
	3.43	5	0	3.539	3.6385	3.5684	3.6065	3.8566
	3.43	5	10	4.1923	4.341	4.3342	4.346	4.0849
	3.43	10	0	3.8767	3.8689	3.7944	3.8752	4.132
	3.43	10	5	4.4269	4.4393	4.4322	4.3774	4.2996
	3.43	10	10	4.6294	4.6592	4.6593	4.6286	4.3861
	3.43	10	15	4.1826	4.2566	4.3198	4.1836	4.2196
	3.43	15	0	4.2495	4.1679	4.204	4.2088	4.693
	3.43	15	5	4.7279	4.82	4.854	4.7755	4.9182
	3.43	15	10	5.0503	5.0916	5.0561	5.0529	5.0258
	3.43	15	15	4.6696	4.703	4.7096	4.66	4.7973
	3.43	20	0	4.7226	4.6503	4.7316	4.7401	5.2515
	3.43	20	5	5.5105	5.4253	5.5111	5.513	5.5699
	3.43	20	10	5.8889	5.7961	5.8586	5.8288	5.6718
	3.43	25	0	5.4549	5.5154	5.5325	5.539	6.0618
	3.43	25	10	6.8253	6.9831	6.955	7.0986	6.5466
	3.43	25	15	6.6779	6.7645	6.6235	6.7906	6.5953
	3.43	30	0	6.791	6.8255	6.7031	6.3642	7.751
	3.43	30	5	7.9667	7.9285	7.9152	7.967	8.3049
	3.43	30	10	8.4853	8.5357	8.4788	8.567	8.316
	3.43	30	15	8.2336	8.3231	8.2089	8.2346	8.2492
	3.43	35	5	9.1141	8.9359	9.1224	8.6622	9.0615
	3.43	35	10	9.462	9.4791	9.5938	9.4653	9.1691
	3.43	35	15	9.0873	9.0961	9.1158	9.0868	9.0391
	3.43	40	5	9.7099	9.8435	9.5985	8.2205	9.5546
	3.43	40	10	10.8167	10.7154	10.5818	9.1011	9.7884
	3.43	40	15	10.2464	10.2184	10.1707	8.6959	9.6736
	3.43	45	0	5.2811	5.3593	5.3371	5.3021	6.0204
	3.43	45	5	6.1173	6.2425	6.2955	6.7522	7.0631
	3.43	45	10	6.599	6.6053	6.6945	7.5012	7.6987
	3.43	50	0	4.5152	4.3638	4.4731	4.1721	5.0545
	3.43	50	5	4.9607	5.0995	4.9557	4.962	5.3887
	3.43	50	15	4.9407	4.9868	5.0129	5.003	5.6358
	3.43	55	0	3.3862	3.3337	3.4022	3.3867	4.7099
	3.43	55	5	3.5763	3.706	3.6271	3.5948	4.8561
	3.43	55	10	3.7944	3.8051	3.717	3.7943	4.8097
	3.43	55	15	3.3383	3.4101	3.4118	3.3386	4.8492
PVA	4	0	0	4	3.9592	3.9811	4.0003	3.8007
	4	0	5	4.6013	4.5632	4.6602	4.6004	3.8968
	4	0	15	4.4557	4.3911	4.3377	4.4555	3.8314
	4	5	0	4.1982	4.1646	4.106	4.1561	3.8687
	4	5	10	5.1597	5.0978	5.0165	5.1591	4.0231

Tables A-1. Obtained E_c from experiments and neural networks for training observations.

Resin type	E_r	%sand	%glass	E_c (GPa)				
				Exp.	FFNN	RBNN	SVM	ALM
	4	5	15	4.7092	4.6619	4.6259	4.7071	3.9494
	4	10	0	4.4106	4.4024	4.3615	4.412	4.2307
	4	10	5	5.0298	5.1338	5.1424	5.0297	4.3426
	4	10	15	4.9868	5.0051	5.0408	5.0282	4.2441
	4	15	0	4.8679	4.7342	4.868	4.8653	4.7266
	4	15	10	6.0828	5.9364	5.8875	6.0821	4.9397
	4	15	15	5.5673	5.529	5.4859	5.5489	4.8237
	4	20	0	5.6188	5.3012	5.5359	5.6172	5.2944
	4	20	5	6.4275	6.2644	6.4513	6.3716	5.4925
	4	20	15	6.4571	6.446	6.5763	6.458	5.5386
	4	25	0	6.3753	6.3349	6.4694	6.6046	6.2599
	4	25	5	7.5661	7.4913	7.6465	7.5652	6.6674
	4	25	10	8.1871	8.1613	8.2138	8.3889	6.5947
	4	25	15	7.7807	7.968	7.8854	7.78	6.5056
	4	30	0	7.8374	7.8783	7.7553	7.489	7.7987
PVA	4	30	10	10.0792	9.9509	9.8197	9.7948	8.1755
	4	35	0	8.8822	9.1164	8.9	7.8053	9.1038
	4	35	5	10.5631	10.3888	10.5569	9.2198	9.1202
	4	35	10	10.8418	11.0276	11.1924	10.5051	9.1826
	4	35	15	10.6245	10.6217	10.6513	9.8523	9.056
	4	40	10	12.4596	12.4698	12.219	9.9536	9.6976
	4	40	15	11.8771	12.0689	11.8353	9.3784	9.5952
	4	45	0	6.1825	6.2744	6.1182	6.1809	6.3094
	4	45	5	7.1191	7.2853	7.266	7.3399	7.2566
	4	45	10	7.7798	7.7336	7.8053	8.2421	7.7183
	4	45	15	7.4583	7.3657	7.5614	7.799	7.2397
	4	50	5	5.8808	5.9096	5.76	5.6932	5.1144
	4	50	10	6.0961	6.1474	6.0502	6.0943	5.2038
	4	50	15	5.936	5.8294	5.8421	5.7838	5.4418
	4	55	0	3.9123	3.8047	3.9711	3.9124	4.7411
	4	55	10	4.321	4.4381	4.38	4.3235	4.8039
	4	55	15	4.1128	4.0168	4.072	4.1138	4.8303

Table A-2. Obtained E_c from experiments and neural networks for testing observations. (Continued)

Resin type	E_r	%sand	%glass	E_c (GPa)				
				Exp.	FFNN	RBNN	SVM	ALM
	1.636	0	15	1.7508	1.8004	1.9141	2.1126	1.8776
	1.636	10	15	2.1247	2.1247	1.8742	2.0401	2.1044
	1.636	20	10	2.7668	2.7231	2.9085	2.7207	2.5751
EPON 828	1.636	25	15	3.1105	3.0738	2.8813	3.4164	3.0806
	1.636	40	0	3.8226	3.704	3.6787	3.2345	3.5
	1.636	40	15	4.7555	4.7846	4.9543	4.1572	4.0859
	1.636	45	15	3.0413	3.1808	2.9428	3.406	2.6812
	1.636	50	10	2.6192	2.4729	2.5973	2.4496	2.4043
	2.463	0	15	2.5745	2.6286	2.7705	2.8015	2.7665
	2.463	5	15	2.9489	2.8331	2.9878	2.9418	2.7988
EPON 862	2.463	15	0	3.037	3.0984	3.0444	3.0301	3.267
	2.463	20	0	3.4213	3.4272	3.3463	3.363	3.7444
	2.463	30	0	4.9297	4.8876	4.7948	4.7337	5.0843
	2.463	35	5	6.5495	6.3992	6.5045	6.5435	6.4195

Table A-2. Obtained E_c from experiments and neural networks for testing observations.

Resin type	E_r	%sand	%glass	E_c (GPa)				
				Exp.	FFNN	RBNN	SVM	ALM
EPON 862	2.463	45	5	4.3986	4.4407	4.5029	5.1228	4.5309
	2.463	50	0	3.225	3.1545	3.2384	2.9348	3.5246
	2.463	55	5	2.7501	2.6629	2.5483	2.6763	3.5744
Epoxy L135i	2.6	0	5	2.9755	2.8577	2.9169	3.0271	2.9074
	2.6	10	5	3.2765	3.3769	3.3508	3.4122	3.2461
	2.6	10	15	3.1787	3.2252	3.2113	3.3427	3.1985
	2.6	15	15	3.7146	3.5519	3.5825	3.6251	3.6334
	2.6	20	15	4.2493	4.0973	4.2482	4.1419	4.0903
	2.6	35	0	5.7097	5.7987	5.8816	5.3134	6.153
	2.6	40	0	6.1966	6.2066	5.9019	4.9669	5.7283
	2.6	40	10	8.3001	8.0934	8.1059	6.8987	6.7008
	2.6	45	10	5.0163	4.9852	5.0325	5.573	5.0313
	2.6	50	0	3.3488	3.3305	3.4193	3.0259	3.8434
	2.6	55	10	2.933	2.8658	2.8142	2.7524	3.7663
LY564	3.43	0	0	3.43	3.4292	3.4324	3.3995	3.7631
	3.43	5	5	4.0077	4.1476	4.1092	4.1211	4.0046
	3.43	5	15	3.9869	3.9536	4.0432	3.8716	3.9208
	3.43	20	15	5.5352	5.4734	5.601	5.4941	5.5744
	3.43	25	5	6.3653	6.465	6.5267	6.6843	6.6344
	3.43	35	0	7.4332	7.7891	7.737	6.7316	8.9812
	3.43	40	0	8.064	8.1542	7.6291	6.3239	8.4897
	3.43	45	15	6.1622	6.2861	6.4203	7.0878	7.5309
	3.43	50	10	5.4649	5.2507	5.2055	5.434	5.6584
PVA	4	0	10	4.7152	4.8082	4.8458	4.8546	3.9485
	4	5	5	4.8292	4.8271	4.7803	4.7723	3.9677
	4	10	10	5.3758	5.4437	5.4305	5.5265	4.3991
	4	15	5	5.6675	5.5581	5.6392	5.5137	4.871
	4	20	10	6.8373	6.7644	6.8713	7.0228	5.575
	4	30	5	9.1921	9.1902	9.1521	8.7122	8.1813
	4	30	15	9.7878	9.7601	9.499	9.1414	8.2542
	4	40	0	9.459	9.3793	8.6876	7.3078	8.7371
	4	40	5	11.3536	11.3325	10.9768	8.7094	9.5234
	4	50	0	5.205	5.0427	5.1444	4.9016	4.9395
	4	55	5	4.3439	4.2742	4.2862	4.3554	4.8348

In addition, tables A-3 and 4 give the obtained σ_{uc} from experiments and neural networks for training and testing observations.

Tables A-3. Obtained σ_{uc} from experiments and neural networks for training observations. (Continued)

Resin type	σ_{ur}	%sand	%glass	σ_{uc} (MPa)				
				Exp.	FFNN	RBNN	SVM	ALM
EPON 828	54.48	0	0	54.477	55.7851	54.3753	28.6071	53.6665
	54.48	0	5	36.3082	35.7848	36.281	30.9171	36.8057
	54.48	0	10	30.6315	32.9579	30.2623	30.6305	30.6278
	54.48	5	0	23.9671	23.6017	23.9385	23.9681	31.8989
	54.48	5	5	20.7432	23.143	22.134	25.3631	26.6449
	54.48	5	10	24.9618	23.4324	23.7432	24.9524	26.9948
	54.48	5	15	18.8838	19.727	20.0715	20.7504	23.4039
	54.48	10	0	18.9885	18.6467	17.8805	20.0495	20.0443
	54.48	10	5	19.9698	20.3107	19.852	20.9314	20.1542

Tables A-3. Obtained σ_{uc} from experiments and neural networks for training observations. (Continued)

Resin type	σ_{ur}	%sand	%glass	σ_{uc} (MPa)				
				Exp.	FFNN	RBNN	SVM	ALM
	54.48	10	10	20.5124	20.9277	20.2429	20.5134	20.8776
	54.48	15	0	17.4221	17.868	18.9854	17.9012	18.3457
	54.48	15	5	20.1246	19.7538	19.9211	18.9475	19.2034
	54.48	15	10	17.567	20.4695	18.9727	18.7055	17.8761
	54.48	15	15	15.9865	17.5942	15.6247	17.0617	15.9565
	54.48	20	0	18.9492	18.0887	17.478	17.8208	18.6015
	54.48	20	5	20.6194	20.0834	19.6531	19.6956	19.1031
	54.48	20	15	18.828	17.7682	18.1349	18.827	18.128
	54.48	25	0	17.1081	19.4391	18.8662	19.1736	19.2334
	54.48	25	5	20.7538	21.8283	21.2736	22.2233	20.6393
	54.48	25	10	21.5984	22.7008	21.8608	22.7783	21.4166
	54.48	30	0	20.4189	21.9521	19.3074	20.6669	21.3748
	54.48	30	5	24.758	25.3528	24.1084	24.759	23.7226
	54.48	30	10	25.6786	27.2426	25.6839	25.6796	25.2638
	54.48	30	15	27.6466	26.0401	27.6297	24.7952	26.3786
EPON 828	54.48	35	0	21.7471	22.4355	22.2766	20.9635	24.0444
	54.48	35	5	29.2842	26.9983	29.5374	25.5543	28.3819
	54.48	35	10	28.2461	28.4251	28.4495	26.6213	27.7278
	54.48	35	15	25.6426	25.8751	26.1514	25.6436	26.3636
	54.48	40	5	33.3239	33.6133	34.0794	23.7196	31.7746
	54.48	40	10	33.0457	32.7273	31.3768	24.6625	31.5073
	54.48	45	0	16.1209	15.9173	14.9302	15.9867	21.8652
	54.48	45	5	19.5845	18.5203	19.6499	19.6182	24.7651
	54.48	45	10	17.2612	17.5912	18.4914	20.2351	23.0804
	54.48	50	0	10.6348	11.6598	10.8134	11.986	12.8481
	54.48	50	5	12.8819	13.05	13.1761	14.6316	14.4276
	54.48	50	15	14.863	12.643	14.0208	14.864	14.9535
	54.48	55	0	8.6975	7.3014	9.1322	8.6985	9.4579
	54.48	55	5	10.4607	11.0092	9.7274	10.4597	10.0063
	54.48	55	10	8.8147	10.9916	8.9898	10.3994	9.0472
	54.48	55	15	10.906	9.6831	11.3177	10.907	10.9876
	93.54	0	0	93.541	93.4378	93.3295	41.0201	88.3401
	93.54	0	5	58.8938	60.3845	59.2767	45.4663	57.9415
	93.54	0	10	53.7847	54.8589	53.3707	43.0103	47.3515
	93.54	5	0	38.8327	39.4758	39.2174	36.147	48.5309
	93.54	5	5	40.1159	38.7513	39.3257	40.053	43.8171
	93.54	5	10	39.343	39.4555	40.3507	38.5643	36.7395
	93.54	10	0	31.7029	30.649	31.7127	31.7039	32.6646
	93.54	10	5	32.7764	33.9836	32.9089	35.3533	31.9062
	93.54	10	10	35.0161	35.1153	34.5275	35.0964	32.3582
EPON 862	93.54	10	15	30.8656	30.2336	30.6482	30.7828	28.9016
	93.54	15	5	31.651	33.3235	31.467	33.338	30.0068
	93.54	15	10	32.0249	34.7433	31.829	34.3984	32.0587
	93.54	15	15	30.2123	30.6104	30.5439	30.4933	29.0847
	93.54	20	5	35.5225	34.184	35.9735	34.7216	32.5291
	93.54	20	10	36.9912	35.8382	37.4358	36.9902	31.2906
	93.54	20	15	33.664	32.4064	33.7427	32.8	31.132
	93.54	25	0	30.504	32.4715	30.1854	31.9404	30.9079
	93.54	25	5	35.3162	37.0186	35.8027	38.4605	33.6806
	93.54	25	10	38.9894	39.2488	37.7578	41.6442	36.9359
	93.54	25	15	36.1733	36.869	35.9251	36.6757	34.2263

Tables A-3. Obtained σ_{uc} from experiments and neural networks for training observations. (Continued)

Resin type	σ_{ur}	%sand	%glass	σ_{uc} (MPa)				
				Exp.	FFNN	RBNN	SVM	ALM
EPON 862	93.54	30	5	45.4836	42.7199	44.5976	42.1733	36.2845
	93.54	30	10	45.8365	46.1767	47.5153	45.8355	43.5178
	93.54	30	15	46.0333	45.2624	46.1211	40.0485	41.1862
	93.54	35	0	41.7144	41.1883	42.5792	34.8866	38.687
	93.54	35	10	50.7261	51.3511	50.0678	46.9509	46.3044
	93.54	35	15	48.9149	48.0933	48.2401	40.7833	45.3263
	93.54	40	0	45.4966	45.6478	44.8976	32.3603	37.2064
	93.54	40	5	56.5135	54.7205	56.0407	40.4256	45.284
	93.54	40	10	55.027	55.159	55.7701	43.603	50.5704
	93.54	40	15	48.7734	50.4038	49.6235	37.7675	47.9391
	93.54	45	0	26.1861	27.0587	26.4718	27.0237	25.3903
	93.54	45	10	32.7848	31.4906	32.6608	36.305	35.7858
	93.54	45	15	30.2193	30.2171	29.1424	31.4801	34.8454
	93.54	50	5	25.5281	24.5602	26.0931	25.5271	22.582
	93.54	50	10	27.1563	26.1053	26.9462	27.1553	25.0587
	93.54	50	15	23.4901	24.8066	24.1808	23.7326	25.4463
	93.54	55	0	12.7127	11.9795	12.3002	14.3428	9.4591
	93.54	55	10	19.814	18.8787	19.5389	18.78	15.3274
	93.54	55	15	16.4939	17.2131	16.5154	16.7753	16.3944
Epoxy L135i	63.8	0	0	63.8	63.044	63.7129	31.5329	60.4584
	63.8	0	10	34.8482	37.3877	35.869	34.6576	34.4867
	63.8	0	15	34.7669	34.9074	34.3802	29.506	33.9833
	63.8	5	0	26.5677	26.4475	27.0692	26.5667	35.0502
	63.8	5	5	28.1749	26.1164	27.2048	28.1759	29.3081
	63.8	5	10	28.2638	26.7326	28.5583	28.6536	29.2627
	63.8	5	15	23.5082	23.1242	23.1002	24.673	27.0945
	63.8	10	0	22.487	20.8013	21.9763	22.4209	22.2481
	63.8	10	10	25.0871	23.9804	24.2814	24.0477	23.3522
	63.8	15	0	21.2966	20.0098	21.3033	20.3168	20.0143
	63.8	15	5	21.6655	22.4806	22.5109	21.6911	20.802
	63.8	15	10	22.649	23.6554	22.711	22.4571	20.8616
	63.8	20	0	21.1077	20.3644	21.3431	20.5809	20.713
	63.8	20	5	24.9714	23.0035	25.3493	23.0355	22.8069
	63.8	20	10	26.1248	24.1942	26.9019	24.2013	23.9409
	63.8	25	0	22.2055	21.9661	22.888	22.4292	21.3095
	63.8	25	5	23.9855	25.0709	24.8856	26.3852	23.6144
	63.8	25	10	28.0289	26.5909	26.5657	28.0299	24.9686
	63.8	25	15	25.0116	24.4151	24.4738	26.0274	23.9627
	63.8	30	0	24.3627	24.9761	24.7499	24.3017	23.0834
	63.8	30	5	31.3086	29.1633	29.8134	29.6172	26.4697
	63.8	30	10	32.9003	31.7583	32.9678	31.6419	28.7577
	63.8	30	15	32.1099	30.9629	31.0439	29.3507	28.1282
	63.8	35	5	32.9729	31.8394	32.7447	30.646	31.3332
	63.8	35	10	34.2071	33.943	33.4305	32.7751	30.9152
	63.8	35	15	30.6413	31.5021	31.5021	30.3359	29.744
	63.8	40	5	37.0211	38.7298	38.199	28.4142	34.1393
	63.8	40	15	33.6935	35.2069	35.6169	28.0163	32.2392
	63.8	45	0	19.5948	18.4032	19.4497	18.2048	20.861
	63.8	45	5	22.3963	21.9215	22.2508	23.3542	24.2909
	63.8	45	15	20.9516	21.276	21.0648	22.8979	22.6738
	63.8	50	5	17.8475	16.0302	17.158	17.1048	16.5144

Tables A-3. Obtained σ_{uc} from experiments and neural networks for training observations. (Continued)

Resin type	σ_{ur}	%sand	%glass	σ_{uc} (MPa)				
				Exp.	FFNN	RBNN	SVM	ALM
Epoxy L135i	63.8	50	10	18.0085	17.4939	17.4705	17.8407	16.8131
	63.8	50	15	16.6689	16.3115	16.1391	16.6699	17.5002
	63.8	55	0	7.7242	8.3836	8.4857	8.703	8.2936
	63.8	55	5	11.6857	12.9163	12.1141	11.6847	10.3264
	63.8	55	15	12.3276	12.2931	11.9723	11.3657	12.0598
LY564	64.1	0	5	39.0245	40.6347	39.0648	34.2603	39.3257
	64.1	0	10	37.4291	37.5401	36.6928	34.7795	34.739
	64.1	0	15	35.054	35.0714	35.2687	29.6493	34.0263
	64.1	5	0	25.7713	26.5484	25.7775	26.6585	35.0758
	64.1	5	10	28.4087	26.8461	28.7279	28.7805	28.9977
	64.1	10	0	20.5449	20.8781	20.7271	22.5125	22.0668
	64.1	10	5	22.4609	23.072	23.0192	23.6132	22.9495
	64.1	10	10	22.8128	24.0844	23.5414	24.1808	23.315
	64.1	10	15	21.3262	20.7481	21.3503	21.3272	21.1618
	64.1	15	0	20.1777	20.0859	20.2497	20.4143	20.0213
	64.1	15	5	21.8033	22.5751	21.1704	21.8043	20.8042
	64.1	15	10	22.5225	23.7628	21.5006	22.6018	20.9588
	64.1	15	15	20.8315	20.9908	21.1488	20.4861	19.7772
	64.1	20	0	20.6901	20.4447	20.6012	20.6911	20.7691
	64.1	20	5	25.3537	23.104	24.2863	23.1645	22.8159
	64.1	20	10	25.4694	24.3101	25.7822	24.3644	23.93
	64.1	25	0	23.2375	22.0544	22.3041	22.5551	21.3796
	64.1	25	10	24.7919	26.7196	25.6457	28.214	24.4588
	64.1	25	15	23.667	24.5536	23.6699	26.1705	23.2726
	64.1	30	0	24.3156	25.0806	24.2722	24.4393	23.1452
	64.1	30	5	29.1469	29.2918	29.0916	29.7809	26.14
	64.1	30	10	31.2069	31.9066	32.1559	31.8416	27.6752
	64.1	30	15	28.7667	31.1205	30.2678	29.5054	27.001
	64.1	35	5	30.8115	32.0007	32.0774	30.8125	31.3487
	64.1	35	10	32.2961	34.1231	32.7519	32.9767	30.7531
	64.1	35	15	32.8246	31.6823	30.9231	30.4951	29.5892
	64.1	40	5	39.9969	38.8967	37.5516	28.5672	34.6856
	64.1	40	10	37.7834	38.6213	38.7947	30.4819	34.1197
	64.1	40	15	36.7074	35.3814	35.22	28.1662	32.6754
	64.1	45	0	18.3042	18.4871	19.1071	18.3052	21.1523
	64.1	45	5	21.2518	22.0329	21.6617	23.4795	24.5056
	64.1	45	10	21.7327	21.4018	20.9227	24.8643	24.6888
	64.1	50	0	14.6172	14.027	13.7537	13.1354	14.762
	64.1	50	5	14.8741	16.1266	16.5403	17.1947	16.7131
	64.1	50	15	14.6985	16.4233	15.4888	16.7622	17.1441
	64.1	55	0	8.2047	8.4213	8.1494	8.7419	9.2455
	64.1	55	5	13.2265	12.977	11.6169	11.7396	10.8915
	64.1	55	10	11.9681	13.5973	12.7754	11.9691	11.3578
	64.1	55	15	11.2939	12.37	11.4308	11.4223	11.2346
PVA	88.4	0	0	88.4	87.3785	88.2184	40.1492	88.3401
	88.4	0	5	58.0149	56.4324	58.1062	44.668	57.8273
	88.4	0	15	47.4431	49.5794	47.7702	36.6392	46.7322
	88.4	5	0	34.9143	36.7892	35.4358	34.9153	45.4063
	88.4	5	10	37.8134	37.1337	37.2791	37.8144	39.3379
	88.4	5	15	32.6754	33.092	32.2104	32.6744	39.8552
	88.4	10	0	30.1812	28.6504	28.7948	30.2798	33.2321

Tables A-3. Obtained σ_{uc} from experiments and neural networks for training observations.

Resin type	σ_{ur}	%sand	%glass	σ_{uc} (MPa)				
				Exp.	FFNN	RBNN	SVM	ALM
PVA	88.4	10	5	33.1177	31.8977	33.9431	33.8328	32.7165
	88.4	10	15	27.9683	28.7226	28.7183	29.6834	29.4094
	88.4	15	0	27.3056	27.6638	28.5215	27.9204	28.5332
	88.4	15	10	33.4942	32.8707	33.8828	33.1125	31.4587
	88.4	15	15	29.1202	29.1549	28.2166	29.1713	28.781
	88.4	20	0	28.4516	28.2811	27.7565	28.4506	29.7471
	88.4	20	5	33.3607	32.1671	31.7839	33.3597	32.3833
	88.4	20	15	31.248	30.7829	31.652	31.5499	31.1316
	88.4	25	0	30.4368	30.4683	31.5889	31.011	31.6609
	88.4	25	5	33.806	34.9086	34.6374	37.3438	33.4372
	88.4	25	10	36.8682	37.1825	37.4614	40.6718	34.7206
	88.4	25	15	35.7192	34.9862	35.6194	35.7202	33.6541
	88.4	30	0	35.0958	34.7494	33.9193	33.6244	34.3946
	88.4	30	10	45.0455	43.8283	44.0191	45.0445	42.2271
	88.4	35	0	37.7368	38.5081	37.8307	34.1695	39.6489
	88.4	35	5	44.2756	45.5733	45.025	42.2702	44.4857
	88.4	35	10	47.5922	48.5065	47.665	46.1568	46.1217
	88.4	35	15	45.4871	45.4741	46.1369	40.4314	45.474
	88.4	40	10	53.4909	52.5752	52.751	42.5687	49.9508
	88.4	40	15	49.0269	48.1396	48.5516	37.4389	48.2122
	88.4	45	0	25.7723	25.6164	25.6488	25.7713	25.538
	88.4	45	5	27.6573	30.7756	28.2249	32.0945	28.0808
	88.4	45	10	30.4597	30.0201	30.8047	34.8575	35.114
	88.4	45	15	29.4036	29.0303	29.9198	30.9528	34.83
	88.4	50	5	21.0814	23.3382	19.9932	23.3265	23.4604
	88.4	50	10	23.2548	24.9817	23.2775	25.2698	25.868
	88.4	50	15	24.0168	23.7417	23.77	22.8847	26.2897
	88.4	55	0	9.7226	11.4795	10.303	12.4537	10.4246
	88.4	55	10	15.4023	18.3416	15.9521	16.5919	16.4383
	88.4	55	15	15.6262	16.7709	15.3432	15.6272	17.405

Table A-4. Obtained σ_{uc} from experiments and neural networks for testing observations. (Continued)

Resin type	σ_{ur}	%sand	%glass	σ_{uc} (MPa)				
				Exp.	FFNN	RBNN	SVM	ALM
EPON 828	54.48	0	15	29.7998	30.0823	26.6042	25.1199	30.2629
	54.48	10	15	17.4121	17.6131	16.2024	17.7242	18.109
	54.48	20	10	19.815	20.7223	20.0234	19.81	18.2583
	54.48	25	15	20.8567	20.0961	22.6467	21.9817	21.8732
	54.48	40	0	25.7495	27.9662	24.7482	19.33	29.5634
	54.48	40	15	29.6896	29.6644	24.0743	23.7888	30.263
	54.48	45	15	17.1096	17.6315	15.6802	19.7169	21.7194
	54.48	50	10	15.8807	14.0616	13.2987	14.8667	13.804
EPON 862	93.54	0	15	53.4591	52.8081	55.9608	36.6798	46.7325
	93.54	5	15	34.4425	35.1894	35.7965	33.3015	37.9233
	93.54	15	0	29.6772	29.5657	38.3288	29.3211	27.6659
	93.54	20	0	28.7298	30.1983	35.1421	29.6492	28.9666
	93.54	30	0	39.2076	36.99	34.4005	34.3574	34.6005
	93.54	35	5	47.7201	48.4129	50.9647	43.3086	44.3661
	93.54	45	5	31.5052	32.3945	33.6723	33.8725	26.9674
	93.54	50	0	23.1285	21.535	17.0385	20.3623	18.1618
	93.54	55	5	18.8902	17.543	19.7225	17.8237	15.051

Table A-4. Obtained σ_{uc} from experiments and neural networks for testing observations.

Resin type	σ_{ur}	%sand	%glass	σ_{uc} (MPa)				
				Exp.	FFNN	RBNN	SVM	ALM
Epoxy L135i	63.8	0	5	41.3754	40.4716	39.3005	34.1546	38.9264
	63.8	10	5	22.6482	22.9788	24.2351	23.5078	23.0271
	63.8	10	15	22.9919	20.6479	21.6152	21.1942	21.0386
	63.8	15	15	19.6567	20.8838	21.8943	20.3572	19.5821
	63.8	20	15	22.7331	21.5253	23.6545	22.3502	22.9722
	63.8	35	0	26.5098	26.3948	26.9822	24.6028	28.884
	63.8	40	0	30.5193	32.0168	29.362	22.4748	32.2933
	63.8	40	10	38.1867	38.4381	39.3833	30.2964	33.7157
	63.8	45	10	21.8601	21.284	21.5681	24.7111	24.435
	63.8	50	0	15.3592	13.9502	14.1092	13.0662	14.3891
	63.8	55	10	13.1852	13.5202	13.3411	11.8986	11.7297
LY564	64.1	0	0	64.1	63.2947	62.3819	31.6266	60.9223
	64.1	5	5	25.0281	26.2206	26.5352	28.2804	29.1457
	64.1	5	15	22.9794	23.239	23.5386	24.813	26.7794
	64.1	20	15	22.2103	21.6465	22.8177	22.4827	22.9126
	64.1	25	5	24.0474	25.1814	24.0443	26.5337	23.4785
	64.1	35	0	27.6596	26.5292	26.5455	24.7413	29.3063
	64.1	40	0	32.4773	32.151	28.9292	22.6002	33.2709
	64.1	45	15	20.78	21.3886	20.5739	23.024	22.9381
	64.1	50	10	19.201	17.6012	16.7255	17.9525	16.7389
PVA	88.4	0	10	52.3844	51.5799	48.35	42.7977	47.3803
	88.4	5	5	38.2215	36.2888	36.2219	38.7993	41.8361
	88.4	10	10	32.2776	33.1728	36.3705	33.9565	32.4077
	88.4	15	5	30.3516	31.3208	29.7869	31.7967	30.2337
	88.4	20	10	33.2876	33.9124	36.688	35.797	31.2878
	88.4	30	5	42.5051	40.3622	40.3825	41.2034	35.8992
	88.4	30	15	41.8101	43.0555	43.0754	39.4508	40.7033
	88.4	40	0	42.5311	43.3462	40.1392	31.4499	38.6923
	88.4	40	5	53.315	52.1517	48.6409	39.0871	45.8187
	88.4	50	0	20.0375	20.3333	16.1733	18.7405	19.4427
	88.4	55	5	17.8948	17.0364	14.54	15.3679	15.6502

References

[1] Czarnecki, L. 1985. The status of polymer concrete. *Concrete International Design Construction,* 7**,** pp. 47-53.

[2] Gorninski, J.P., Dal Molin, D.C. and Kazmierczak, C.S. 2007. Comparative assessment of isophtalic and orthophtalic polyester polymer concrete: Different costs, similar mechanical properties and durability. *Construction and Building Materials,* 21 (3)**,** pp. 546-555.

[3] Hashemi, M.J., Jamshidi, M. and Aghdam, J.H. 2018. Investigating fracture mechanics and flexural properties of unsaturated polyester polymer concrete (up-pc). *Construction and Building Materials,* 163**,** pp. 767-775.

[4] Alzeebaree, R., Çevik, A., Nematollahi, B., Sanjayan, J., Mohammedameen, A. and Gülşan, M.E. 2019. Mechanical properties and durability of unconfined and confined geopolymer concrete with fiber reinforced polymers exposed to sulfuric acid. *Construction and Building Materials,* 215**,** pp. 1015-1032.

[5] Agavriloaie, L., Oprea, S., Barbuta, M. and Luca, F. 2012. Characterisation of polymer concrete with epoxy polyurethane acryl matrix. *Construction and Building Materials,* 37**,** pp. 190-196.

[6] Abdulla, A.I., Razak, H.A., Salih, Y.A. and Ali, M.I. 2016. Mechanical properties of sand modified resins used for bonding CFRP to concrete substrates. *International Journal of*

Sustainable Built Environment, 5 (2), pp. 517-525.
[7] Dudek, D. and Kadela, M. 2016. Pull-out strength of resin anchors in non-cracked and cracked concrete and masonry substrates. *Procedia Engineering,* 161, pp. 864-867.
[8] Ferrier, E., Rabinovitch, O. and Michel, L. 2016. Mechanical behavior of concrete–resin/adhesive–FRP structural assemblies under low and high temperatures. *Construction and Building Materials,* 127, pp. 1017-1028.
[9] Aslani, F., Gunawardena, Y. and Dehghani, A. 2019. Behaviour of concrete filled glass fibre-reinforced polymer tubes under static and flexural fatigue loading. *Construction and Building Materials,* 212, pp. 57-76.
[10] Hasan, H.A., Sheikh, M.N. and Hadi, M.N.S. 2019. Maximum axial load carrying capacity of fibre reinforced-polymer (FRP) bar reinforced concrete columns under axial compression. *Structures,* 19, pp. 227-233.
[11] Jirawattanasomkul, T., Ueda, T., Likitlersuang, S., Zhang, D., Hanwiboonwat, N., Wuttiwannasak, N. and Horsangchai, K. 2019. Effect of natural fibre reinforced polymers on confined compressive strength of concrete. *Construction and Building Materials,* 223, pp. 156-164.
[12] Kwon, S., Ahn, S., Koh, H.-I. and Park, J. 2019. Polymer concrete periodic meta-structure to enhance damping for vibration reduction. *Composite Structures,* 215, pp. 385-390.
[13] Aggarwal, L.K., Thapliyal, P.C. and Karade, S.R. 2007. Properties of polymer-modified mortars using epoxy and acrylic emulsions. *Construction and Building Materials,* 21 (2), pp. 379-383.
[14] Bărbuţă, M., Harja, M. and Baran, I. 2010. Comparison of mechanical properties for polymer concrete with different types of filler. *Journal of Materials in Civil Engineering,* 22 (7), pp. 696-701.
[15] Harja, M., Barbuta, M. and Rusu, L. 2009. Obtaining and characterization of the polymer concrete with fly ash. *Journal of Applied Sciences,* 9 (1), pp. 88-96.
[16] Kurugöl, S., Tanaçan, L. and Ersoy, H.Y. 2008. Young's modulus of fiber-reinforced and polymer-modified lightweight concrete composites. *Construction and Building Materials,* 22 (6), pp. 1019-1028.
[17] Abdel-Fattah, H. and El-Hawary, M.M. 1999. Flexural behavior of polymer concrete. Construction *and Building Materials,* 13 (5), pp. 253-262.
[18] Komendant, J., Nicolayeff, V., Polivka, M. and Pirtz, D. 1978. Effect of temperature, stress level, and age at loading on creep of sealed concrete. *ACI SP,* 55, pp. 55–82.
[19] Guo, L.-P., Carpinteri, A., Roncella, R., Spagnoli, A., Sun, W. and Vantadori, S. 2009. Fatigue damage of high performance concrete through a 2d mesoscopic lattice model. *Computational Materials Science,* 44 (4), pp. 1098-1106.
[20] Shahbeyk, S., Hosseini, M. and Yaghoobi, M. 2011. Mesoscale finite element prediction of concrete failure. *Computational Materials Science,* 50 (7), pp. 1973-1990.
[21] Słowik, M. 2011. Numerical analysis of the width of fracture process zone in concrete beams. *Computational Materials Science,* 50 (4), pp. 1347-1352.
[22] Zhou, X.Q. and Hao, H. 2008. Modelling of compressive behaviour of concrete-like materials at high strain rate. *International Journal of Solids and Structures,* 45 (17), pp. 4648-4661.
[23] Oh, B.H., Han, S.H., Kim, Y.S., Lee, B.C. and Shin, H.S. 1997. Mechanical properties of polymer concrete and fiber reinforced polymer concrete. *Polymers in Concretes* pp. 483–492.
[24] Vipulanandan, C. and Dharmarajan, N. 1988. Effect of temperature on the fracture properties of epoxy polymer concrete. *Cement and Concrete Research,* 18 (2), pp. 265-276.
[25] Avci, A., Arikan, H. and Akdemir, A. 2004. Fracture behavior of glass fiber reinforced polymer composite. *Cement and Concrete Research,* 34 (3), pp. 429-434.
[26] Vipulanandan, C. and Mebarkia, S. 1996. Flexural and fracture properties of glass fiber reinforced polyester polymer concrete. *ACI SP* 166 (1), pp. 1-16.
[27] Arikan, H., Avci, A. and Akdemir, A. 2004. Fracture behaviour of steel fibre reinforced polymer composite. *Polymer Testing,* 23 (6), pp. 615-619.
[28] Haidar, M., Ghorbel, E. and Toutanji, H. 2011. Optimization of the formulation of micro-polymer concretes. *Construction and Building Materials,* 25 (4), pp. 1632-1644.
[29] Jafari, K., Tabatabaeian, M., Joshaghani, A. and Ozbakkaloglu, T. 2018. Optimizing the mixture design of polymer concrete: An experimental investigation. *Construction and Building Materials,* 167, pp. 185-196.
[30] Andreassen, E. and Andreasen, C.S. 2014. How to determine composite material properties using numerical homogenization. *Computational Materials Science,* 83, pp. 488-495.
[31] Cramer, A.D., Challis, V.J. and Roberts, A.P. 2016. Microstructure interpolation for macroscopic design. *Structural and*

Multidisciplinary Optimization, 53 (3), pp. 489-500.
[32] Akbari, A., Kerfriden, P. and Bordas, S. 2018. On the effect of grains interface parameters on the macroscopic properties of polycrystalline materials. *Computers & Structures,* 196, pp. 355-368.
[33] Ahn, S., Jeon, E.-B., Koh, H.-I., Kim, H.-S. and Park, J. 2016. Identification of stiffness distribution of fatigue loaded polymer concrete through vibration measurements. *Composite Structures,* 136, pp. 11-15.
[34] Toufigh, V., Hosseinali, M. and Shirkhorshidi, S.M. 2016. Experimental study and constitutive modeling of polymer concrete's behavior in compression. *Construction and Building Materials,* 112, pp. 183-190.
[35] Bulut, H.A. and Şahin, R. 2017. A study on mechanical properties of polymer concrete containing electronic plastic waste. *Composite Structures,* 178, pp. 50-62.
[36] Jafari, K. and Toufigh, V. 2017. Experimental and analytical evaluation of rubberized polymer concrete. *Construction and Building Materials,* 155, pp. 495-510.
[37] Shokrieh, M.M., Rezvani, S. and Mosalmani, R. 2017. Mechanical behavior of polyester polymer concrete under low strain rate loading conditions. *Polymer Testing,* 63, pp. 596-604.
[38] Fernández-Ruiz, M.A., Gil-Martín, L.M., Carbonell-Márquez, J.F. and Hernández-Montes, E. 2018. Epoxy resin and ground tyre rubber replacement for cement in concrete: Compressive behaviour and durability properties. *Construction and Building Materials,* 173, pp. 49-57.
[39] Hassani Niaki, M., Fereidoon, A. and Ghorbanzadeh Ahangari, M. 2018. Experimental study on the mechanical and thermal properties of basalt fiber and nanoclay reinforced polymer concrete. *Composite Structures,* 191, pp. 231-238.
[40] Heidari-Rarani, M. and Bashandeh-Khodaei-Naeini, K. 2018. Micromechanics based damage model for predicting compression behavior of polymer concretes. *Mechanics of Materials,* 117, pp. 126-136.
[41] Fischer, J., Bradler, P.R., Schmidtbauer, D., Lang, R.W. and Wan-Wendner, R. 2019. Long-term creep behavior of resin-based polymers in the construction industry. *Materials Today Communications,* 18, pp. 60-65.
[42] Shabani, M.O. and Mazahery, A. 2012. Artificial intelligence in numerical modeling of nano sized ceramic particulates reinforced metal matrix composites. *Applied Mathematical Modelling,* 36 (11), pp. 5455-5465.
[43] Macabenta Lazo, E. and Pepard Mendoza Rinchon, J. 2018. Hybrid artificial intelligence-based bond strength model of CFRP-lightweight concrete composite. *MATEC Web Conf.,* 192, pp. 02018.
[44] Shouraki, S.B. and Honda, N. 1999. Recursive fuzzy modeling based on fuzzy interpolation. *JACIII,* 3 (2), pp. 114-125.
[45] Bahrpeyma, F., Zakerolhoseini, A. and Haghighi, H. 2015. Using ids fitted q to develop a real-time adaptive controller for dynamic resource provisioning in cloud's virtualized environment. *Applied Soft Computing,* 26, pp. 285-298.
[46] Murakami, M. 2008. *Practicality of modeling systems* using *the ids method: Performance investigation and hardware implementation.* Ph.D., The University of Electro-Communications.
[47] Firouzi, M. and Shouraki, S.B. 2011. Performance evaluation of active learning method in classification problems. *3rd International Conference on* Machine *Learning and Computing (ICMLC 2011).* Singapore.
[48] Firouzi, M., Shouraki, S.B. and Rostami, M.G. Spiking neural network ink drop spread, spike-ids. *In:* Yamaguchi, Y., ed. Advances in Cognitive Neurodynamics (III), 2013// 2013 Dordrecht. Springer Netherlands, pp. 59-68.
[49] Firouzi, M., Shouraki, S.B. and Afrakoti, I.E.P. 2014. Pattern analysis by active learning method classifier. *Journal of Intelligent & Fuzzy Systems,* 26, pp. 49-62.
[50] Javadian, M., Bagheri Shouraki, S. and Sheikhpour Kourabbaslou, S. 2017. A novel density-based fuzzy clustering algorithm for low dimensional feature space. *Fuzzy Sets and Systems,* 318, pp. 34-55.
[51] Javadian, M. and Shouraki, S.B. 2017. Ualm: Unsupervised active learning method for clustering low-dimensional data. *Journal of Intelligent & Fuzzy Systems,* 73 (3), pp. 2393-2411.
[52] Firouzi, M., Shouraki, S.B. and Conradt, J. Sensorimotor control learning using a new adaptive spiking neuro-fuzzy machine, spike-ids and stdp. *In:* Wermter, S., Weber, C., Duch, W., Honkela, T., Koprinkova-Hristova, P., Magg, S., Palm, G. and Villa, A.E.P., eds. Artificial Neural Networks and Machine Learning – ICANN 2014, 2014// 2014 Cham. Springer International Publishing, pp. 379-386.
[53] Sakurai, Y. 2005. *A study of the learning* control *method using pbalm-a nonlinear*

modeling method. The University of Electro-Communications.

[54] Shahdi, S.A. and Shouraki, S.B. 2002. Supervised active learning method as an intelligent linguistic controller and its hardware implementation. *2nd IASTEAD International Conference on Artificial Intelligence and Applications (AIA'02).* Malaga, Spain.

[55] Merrikh-Bayat, F., Shouraki, S.B. and Rohani, A. 2011. Memristor crossbar-based hardware implementation of the ids method. *IEEE Transactions on Fuzzy Systems,* 19 (6)**,** pp. 1083-1096.